

SCAPS Modeling of CMTS Solar Cell with ZrS₂ Buffer Layer

T.A. CHOWDHURY*

Faculty of Department of Electrical & Electronic Engineering, Ahsanullah University of Science & Technology, Dhaka, Bangladesh

Received: 27.10.2023 & Accepted: 21.12.2023

Doi: [10.12693/APhysPolA.145.215](https://doi.org/10.12693/APhysPolA.145.215)

*e-mail: towhid6789@yahoo.com

The aim of this work is to study the photovoltaic performance of CMTS-based solar cell using solar cell capacitance simulator-1D. The use of ZrS₂ as a buffer layer for CMTS-based solar cell is the novelty of this work. The impact of several parameters such as thickness, defect density, electron affinity, and doping concentration on the cell performances is investigated to improve cell performance. It is observed that these parameters impact significantly the solar cell performance. The optimized solar cell obtained an efficiency of 31.54% with an open-circuit voltage of 0.99 V, short-circuit current density of 36.44 mA/cm², and fill factor of 87.69%. The results suggest guidelines for developing low-cost and highly efficient CMTS thin-film solar cells.

topics: CMTS (Cu₂MnSnS₄), ZrS₂, solar cell, solar cell capacitance simulator-1D (SCAPS-1D)

1. Introduction

Solar cells are a promising renewable energy source as they are an environmentally eco-friendly method to reduce CO₂ emissions and satisfy the demand for green energy [1–3]. Extensive research is being conducted on copper-based quaternary chalcogenide semiconductors as a cost-effective substitute to conventional absorber materials in solar cells due to their direct bandgap and abundance in availability [4–6]. Among them, copper zinc tin sulfide (Cu₂ZnSnS₄, i.e., CZTS), copper zinc tin selenide (Cu₂ZnSnSe₄, i.e., CZTSe), and sulfur-selenium alloy (Cu₂ZnSn(S_xSe_{1-x})₄, i.e., CZTSSe) based thin-film solar cells have been widely studied [7–11]. Due to a tunable bandgap between 1.4–1.5 eV, CZTS is a suitable solar cell absorber layer [12–14]. Antisite defects present in CZTS due to similar atomic size of zinc and copper atoms have hindered their efficiency improvement in recent years [15–18]. The zinc replacement in CZTS with various cations results in materials that have similar optical characteristics to CZTS material [19–23]. Among them, copper manganese tin sulfide (Cu₂MnSnS₄, i.e., CMTS) is a promising material due to its low cost, nontoxicity, high absorption coefficient (> 10⁴ cm⁻¹), and tunable bandgap between 1.2–1.5 eV [24–29]. Electro deposition [30], chemical vapor deposition [31], sol-gel [32], and thermal evaporation [33] are some of the methods used to deposit CMTS thin films. The numerical efficiency in the range of 16.5–20.26% was obtained

in ZnO:Al/i-ZnO/buffer (ZnO, ZnS, CdS)/CMTS and i-ZnO/CdS/CMTS solar cell [34, 35]. However, an in-depth analysis of the CMTS absorber layer with a nontoxic buffer layer and favorable metal contact has not been performed.

Recently, transition metal dichalcogenides (TMDCs) have been used for various applications, especially in photodetectors [36, 37] and solar cells [38] instead of conventional materials due to large band-edge excitation produced by *d-d* transition situated at a metal site [2]. Zirconium disulfide (ZrS₂), a group IV of TMDCs, shows a low lattice mismatch with absorber materials due to the van der Waals force [38, 39]. The high absorption coefficient, quasi-2D characteristic, and tunable bandgap energy in the range of 1.2–2.2 eV [38, 40, 41] make ZrS₂ applicable in various opto-electronic devices [42, 43]. Various methods, such as sputtering [44], atomic layer deposition [45], and chemical vapor transport [46], are used to deposit ZrS₂ thin film. ZrS₂, a TMDC material, builds heterostructures by facilitating vertical stacking of several TMDC materials without the requirement of lattice matching due to the absence of dangling bonds. Solar cells of high efficiency can be obtained by combining p-type semiconductors such as CMTS with n-type ZrS₂ with appropriate energy level alignment.

The present work explores a detailed numerical simulation of AZO/ZrS₂/CMTS solar cell, where CMTS is used as an absorber layer, and ZrS₂ is used as a novel buffer layer, using solar cell capacitance

TABLE I

Input data used in the simulated CMTS/ZrS₂/AZO thin-film solar cell.

| Parameter | Unit | CMTS [35] | ZrS ₂ [38] | AZO [52–54] |
|---|--------------------------------|----------------------|-----------------------|----------------------|
| thickness | [μm] | 1 | 0.05 | 0.3 |
| bandgap | [eV] | 1.2 | 1.7 | 3.3 |
| electron affinity | [eV] | 4.35 | 4.7 | 4.52 |
| dielectric permittivity | | 7.6 | 16.4 | 9 |
| conduction band effective density of states | [cm^{-3}] | 2.2×10^{18} | 1.8×10^{19} | 2.2×10^{18} |
| valence band effective density of states | [cm^{-3}] | 1.8×10^{19} | 2.2×10^{19} | 1.8×10^{19} |
| electron thermal velocity | [cm/s] | 1×10^7 | 1×10^7 | 1×10^7 |
| hole thermal velocity | [cm^{-1}] | 1×10^7 | 1×10^7 | 1×10^7 |
| electron mobility | [$\text{cm}^2/(\text{V s})$] | 0.16 | 300 | 100 |
| hole mobility | [$\text{cm}^2/(\text{V s})$] | 0.16 | 30 | 25 |
| shallow uniform donor density N_D | [cm^{-3}] | 0 | 1×10^{18} | 1×10^{20} |
| shallow uniform acceptor density N_A | [cm^{-3}] | 1×10^{16} | 0 | 0 |

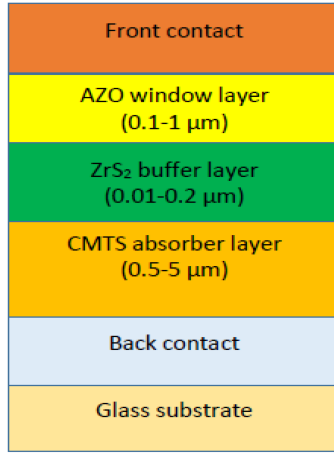
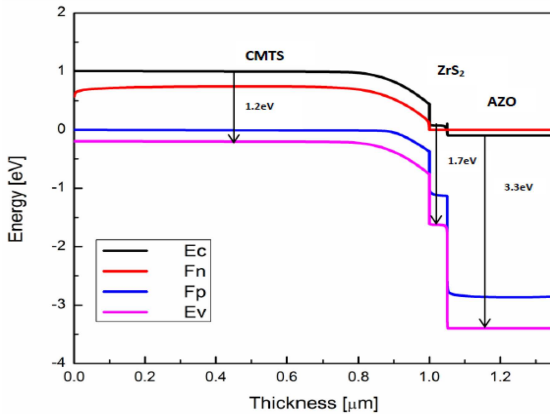
Fig. 1. Representation of the CMTS/ZrS₂/AZO solar cell.

Fig. 2. Energy band diagram.

simulator (SCAPS-1D) software. Al-doped ZnO is used as a window layer in simulation instead of pure ZnO as Al doping causes low resistivity, reduction in defect states, high transmittance and car-

rier mobility, and as a result, enhances solar cell performance [47–49]. The influence of various parameters such as absorber layer thickness, acceptor concentration, electron affinity, bulk defect density of absorber, buffer layer thickness, donor concentration, bulk defect density of buffer, window layer thickness, bulk defect density of window, and interfacial defect density on the solar cell performance parameters open-circuit voltage (V_{oc}), short-circuit current density (J_{sc}), fill factor (FF), and efficiency (η) are investigated and optimized to obtain the highest efficiency of the proposed solar cell. The results of this study will give a guideline for the experimental production of high-performance CMTS-based solar cells.

2. Simulation methodology and device structure

Solar cell capacitance simulator (SCAPS-1D) developed at the University of Gent, Belgium, is used to design and simulate the proposed solar cell. The essential charge carrier transport equations, such as Poisson's equation and electron and hole continuity equations are solved numerically by this software [50]. This software helps to analyze and simulate the J - V characteristic curve, spectral response (QE) curve, AC characteristics (C - V and C - f), open-circuit voltage (V_{oc}), fill factor, short-circuit current density (J_{sc}), and efficiency of solar cells [51].

Figure 1 shows the CMTS/ZrS₂/AZO solar cell structure that includes p-type CMTS as an absorber, n-type ZrS₂ as a buffer layer, and Al-doped ZnO (AZO) as a window layer. The parameter values used to simulate the proposed solar cell structure are listed in Table I (see also [35, 38, 52–54]). The device performance is simulated at 300 K operating temperature under air mass AM 1.5G solar irradiance with standard illumination (1000 W/m^2).

3. Results and discussion

3.1. Energy band diagram

The energy band diagram obtained from SCAPS for the simulated CMTS/ ZrS_2 /AZO solar cell is shown in Fig. 2. According to the Shockley–Queisser limit, the maximum efficiency of 32.5% using an AM 1.5 G spectrum is theoretically possible to obtain from a CMTS single-junction solar cell due to absorber layer bandgap of 1.2 eV [55].

3.2. Impact of CMTS absorber layer thickness

The impact of the CMTS absorber layer thickness is investigated by changing the absorber layer thickness from 0.5 to 5 μm . The simulation results are shown in Fig. 3. All the solar cell parameters increase with the increase in absorber layer thickness. Too thin the absorber layer results in a lower generation rate of electron–hole as it is not adequate enough to absorb all incident light. As the absorber layer thickness is increased, the increase in the optical path causes greater photon absorption in the absorber layer [56], and thus, the efficiency

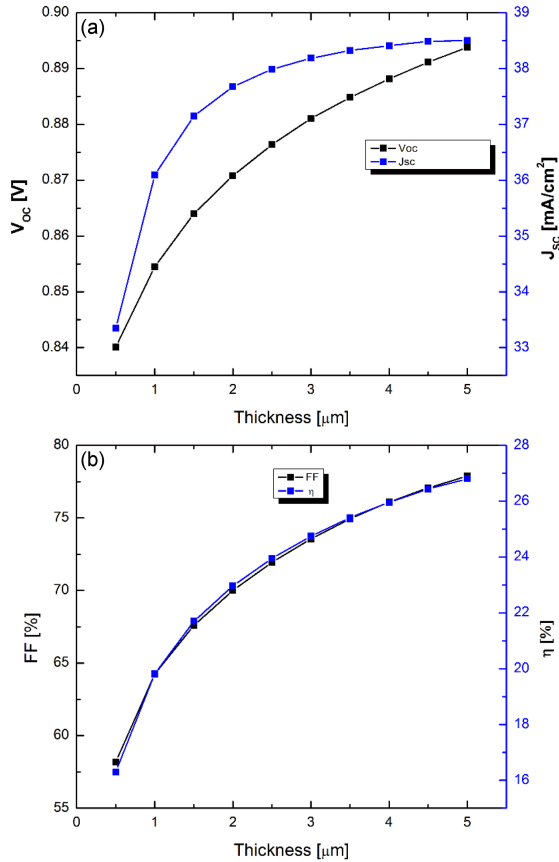


Fig. 3. The impact of CMTS absorber layer thickness on solar cell performance (a) V_{oc} and J_{sc} variation, (b) FF and η variation.

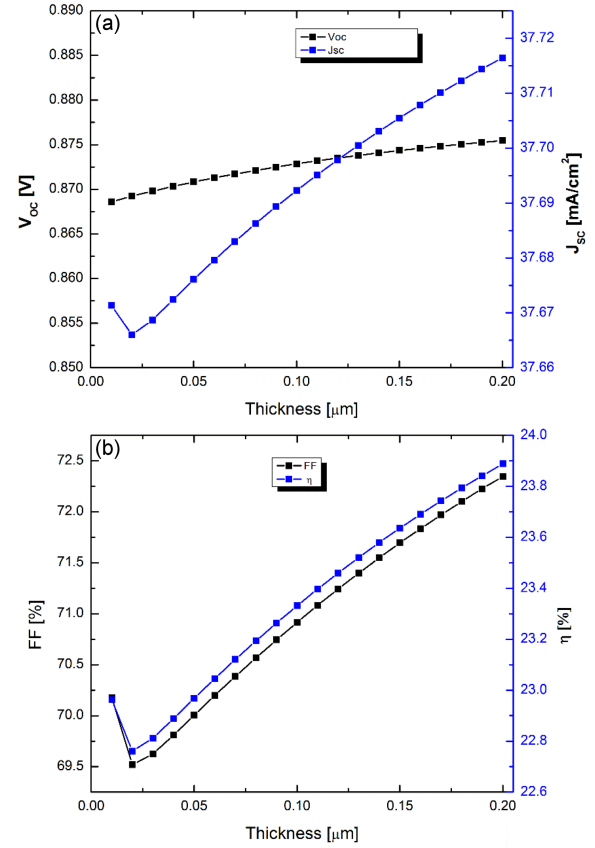


Fig. 4. The impact of ZrS_2 buffer layer thickness on solar cell performance (a) V_{oc} and J_{sc} variation, (b) FF and η variation.

increases. As the thickness is further increased, the increased recombination rate slows the increase in efficiency. The efficiency increases as absorber layer thickness is increased in the considered range. The efficiency is 16.3% when the absorber layer thickness is 0.5 μm . The efficiency increases by 15.95% from 19.81 to 22.97% as absorber layer thickness is increased from 1 to 2 μm . When absorber layer thickness is varied from 2 to 3 μm , the efficiency increases by 7.75% from 22.97 to 24.75%. The efficiency increment is 4.89% (from 24.75 to 25.96%) and 3.24% (from 25.96 to 26.8%) as absorber layer thickness is increased from 3 to 4 μm and from 4 to 5 μm , respectively. The efficiency increases at a slow rate as absorber layer thickness is increased by 1 μm above 2 μm in the considered range. Therefore, to reduce CMTS material usage and production cost, the chosen absorber layer thickness is 2 μm , and various layer parameters have been optimized to improve efficiency.

3.3. Impact of ZrS_2 buffer layer thickness

The impact of the ZrS_2 buffer layer thickness is investigated, and the simulation results are shown in Fig. 4. The buffer layer thickness is altered from 0.01 to 0.2 μm . The buffer layer should ideally be as

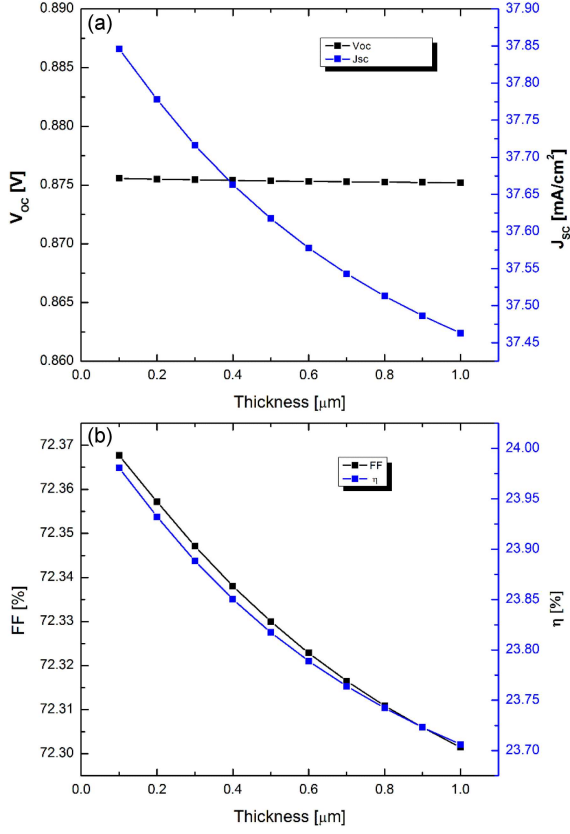


Fig. 5. The impact of AZO window layer thickness on solar cell performance (a) V_{oc} and J_{sc} variation, (b) FF and η variation.

thin as possible to enhance the device's performance as it increases photogenerated electron collection by front contact. The value of V_{oc} , J_{sc} , and FF increases from 0.869 V, 37.67 mA/cm^2 , and 70.18% to 0.875 V, 37.716 mA/cm^2 , and 72.35%, respectively, as the buffer layer thickness is increased from 0.01 to 0.2 μm . Therefore, the combined effect of these parameters causes efficiency to increase from 22.96 to 23.9% as the buffer layer thickness is increased from 0.01 to 0.2 μm . An increase in the number of ionizing atoms with an increase in the thickness of the ZrS_2 buffer layer results in an increased number of photogenerated electrons [57]. As a result, efficiency increases with an increase in ZrS_2 layer thickness. The chosen optimal ZrS_2 buffer layer thickness is 0.2 μm .

3.4. Impact of AZO window layer thickness

Figure 5 shows the simulation results of AZO window layer thickness variation from 0.1 to 1 μm . The value of V_{oc} remains unaltered, but both J_{sc} and FF decrease with an increase in AZO window layer thickness. As a result, η decreases from 23.98 to 23.71% as AZO window layer thickness is increased from 0.1 to 1 μm . The carriers need to travel a distance greater than the carriers' diffusion length

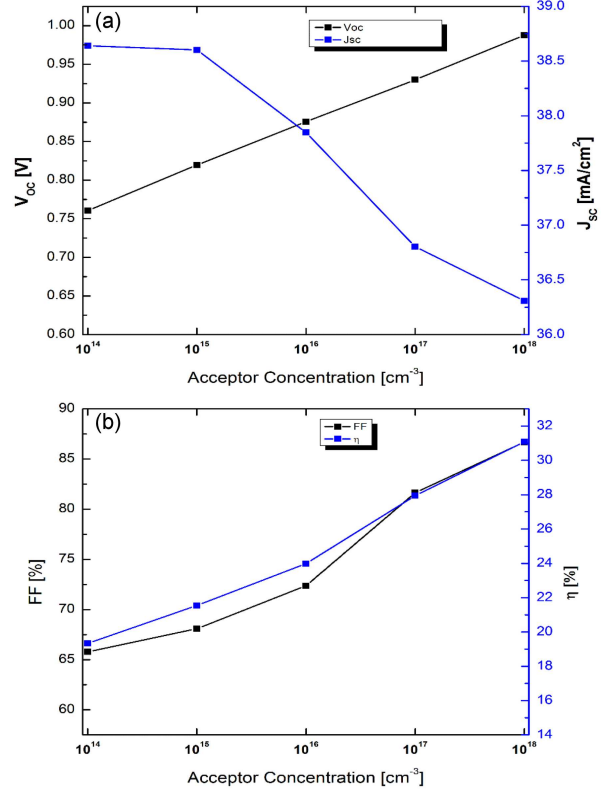


Fig. 6. The impact of CMTS absorber layer acceptor concentration on solar cell performance (a) V_{oc} and J_{sc} variation, (b) FF and η variation.

to reach front contact, thus enhancing the recombination rate and causing efficiency to decline as window layer thickness is increased [57]. The AZO window layer thickness of 0.1 μm will result in maximum solar cell efficiency.

3.5. Impact of CMTS absorber layer acceptor concentration

The influence of CMTS absorber layer acceptor concentration on solar cell performance is shown in Fig. 6. The acceptor concentration is altered from 10^{14} to 10^{18} cm^{-3} . The value of J_{sc} decreases due to the high recombination rate, but both FF and V_{oc} increase with the increase in acceptor concentration in the considered range. The efficiency increases from 19.33% to 31.08% as the absorber layer acceptor concentration is changed from 10^{14} cm^{-3} to 10^{18} cm^{-3} . Low absorber layer doping concentration causes a large number of carrier recombinations in the buffer layer due to the shifting of the depletion region towards the p-region. As absorber layer acceptor concentration increases, the depletion region moves further towards the n-region, resulting in more separation of photogenerated electron-hole pairs by an electric field in the n-region, which contributes to the photocurrent and increases efficiency [56]. The optimal value of the

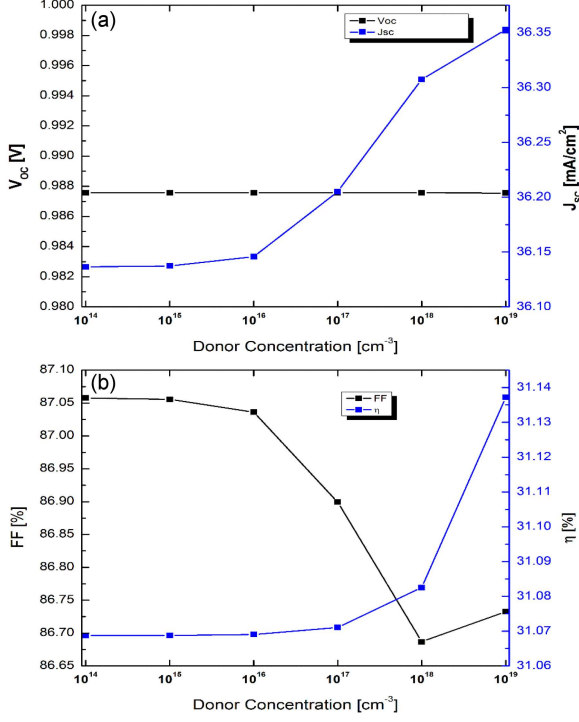


Fig. 7. The impact of ZrS₂ buffer layer donor concentration on solar cell performance (a) V_{oc} and J_{sc} variation, (b) FF and η variation.

absorber layer acceptor concentration is 10^{18} cm^{-3} , which is well within the acceptor density of 10^{19} cm^{-3} found for the CMTS absorber layer obtained in previous studies [58–60].

3.6. Impact of ZrS₂ buffer layer donor concentration

Simulation results obtained by changing ZrS₂ buffer layer donor concentration from 10^{14} to 10^{19} cm^{-3} are shown in Fig. 7. The value of V_{oc} is almost unaffected, and J_{sc} increases as buffer layer donor concentration is increased. The value of FF decreases from 87.06 to 86.68% as donor concentration is changed from 10^{14} to 10^{18} cm^{-3} . Then, the value of FF increases slightly to 86.73% as donor concentration is increased to 10^{19} cm^{-3} . The combined impact of V_{oc} , J_{sc} , and FF causes efficiency to increase from 31.07 to 31.14% as buffer layer donor concentration is increased from 10^{14} to 10^{19} cm^{-3} . The photogenerated carrier separation is increased with an increase in buffer layer donor concentration as the depletion region shifts towards the absorber layer, and the electric field is increased on the CMTS/ZrS₂ junction. Thus, contacts collect an increased number of carriers, and efficiency increases [56, 61, 62]. The optimal value of the buffer layer donor concentration is 10^{19} cm^{-3} . This chosen value is consistent with the donor concentration for the ZrS₂ buffer material used in the previous report [2]. At donor

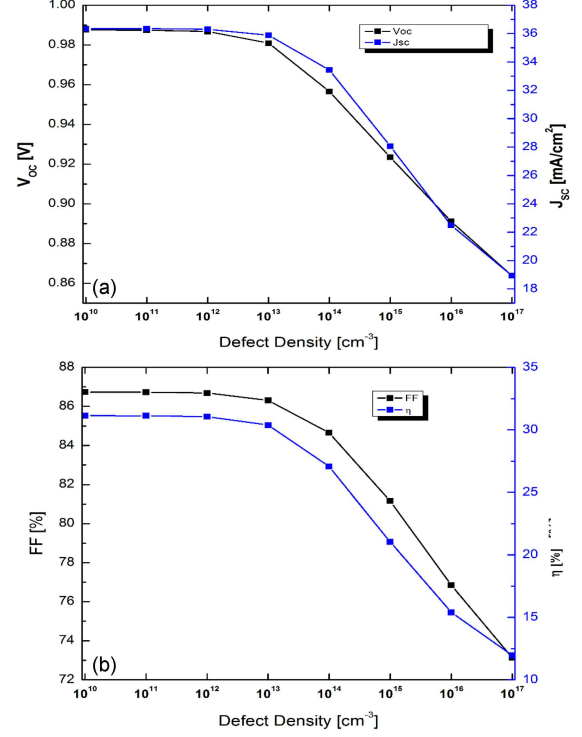


Fig. 8. The impact of CMTS absorber layer defect density on solar cell performance (a) V_{oc} and J_{sc} variation, (b) FF and η variation.

concentrations $> 10^{17} \text{ cm}^{-3}$, ZrS₂ behaves as a degenerate semiconductor, which enhances the conductivity of the solar cell [63].

3.7. Impact of CMTS absorber layer defect density

To analyze the impact of CMTS absorber layer defect density on solar cell performance, the defect density is varied from 10^{10} to 10^{17} cm^{-3} . The obtained simulation results are shown in Fig. 8. Single-donor type bulk defect is used for the absorber layer. The proposed solar cell has an efficiency close to 31.14% up to a defect density of 10^{13} cm^{-3} . Then efficiency declines. The efficiency decreases to 11.96% as defect density is increased to 10^{17} cm^{-3} . Thus, CMTS absorber layer defect density needs to be minimized below 10^{13} cm^{-3} . The Shockley–Read–Hall recombination rate increases with an increase in absorber layer defect density, which traps photogenerated carriers and causes a reduction in their number by decreasing their lifetime. As a result, V_{oc} , J_{sc} , FF, and efficiency decrease [64, 65]. Too low absorber defect density is impossible to achieve in practical cases [66]. Therefore, the optimal absorber defect density $< 10^{13} \text{ cm}^{-3}$ is feasible. It has been observed that a defect density level of 10^{12} – 10^{15} cm^{-3} is feasible in metal chalcogenide-based thin films [67, 68].

3.8. Impact of ZrS₂ buffer layer defect density

The impact of ZrS₂ buffer layer defect density on solar cell performance is also explored. The defect density is varied from 10^{10} to 10^{18} cm⁻³. Figure 9 shows the simulation results obtained. Single-acceptor type bulk defect is used for the buffer layer. The efficiency of around 31.14% of the proposed solar cell is unaffected up to the defect density of 10^{16} cm⁻³. The efficiency decreases to 23.1% as defect density is increased to 10^{18} cm⁻³. It is observed that due to the thinner thickness of the buffer layer compared to the absorber layer, buffer layer defect density has less impact on solar cell performance [3]. As a result, the ZrS₂ buffer layer defect density needs to be minimized below 10^{16} cm⁻³, which is within the defect density tolerance range for the ZrS₂ layer, which is between 10^{12} to 10^{18} cm⁻³, obtained in previous research work [69]. An increase in buffer layer defect density increases the Shockley–Read–Hall recombination rate, which decreases the efficiency of the solar cell [64].

3.9. Impact of AZO window layer defect density

The impact of AZO window layer defect density on solar cell performance is investigated by altering defect density from 10^{10} to 10^{20} cm⁻³. The simulation results are shown in Fig. 10. Single-acceptor type bulk defect is used for the window layer.

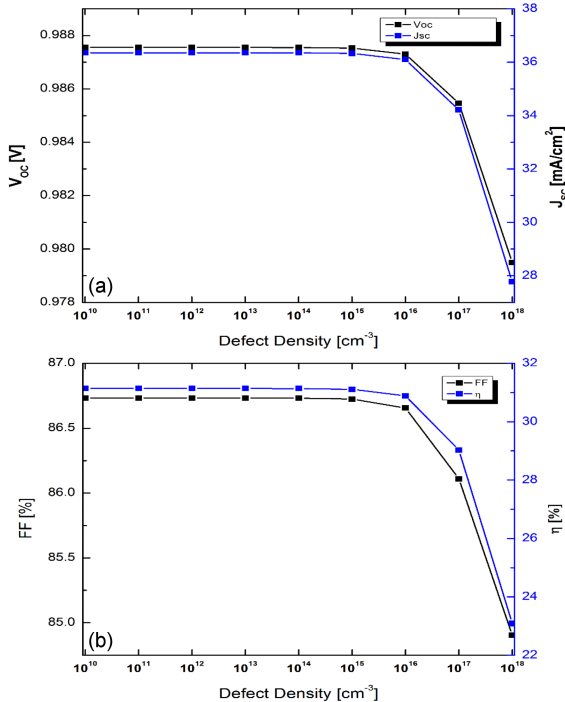


Fig. 9. The impact of ZrS₂ buffer layer defect density on solar cell performance (a) V_{oc} and J_{sc} variation, (b) FF and η variation.

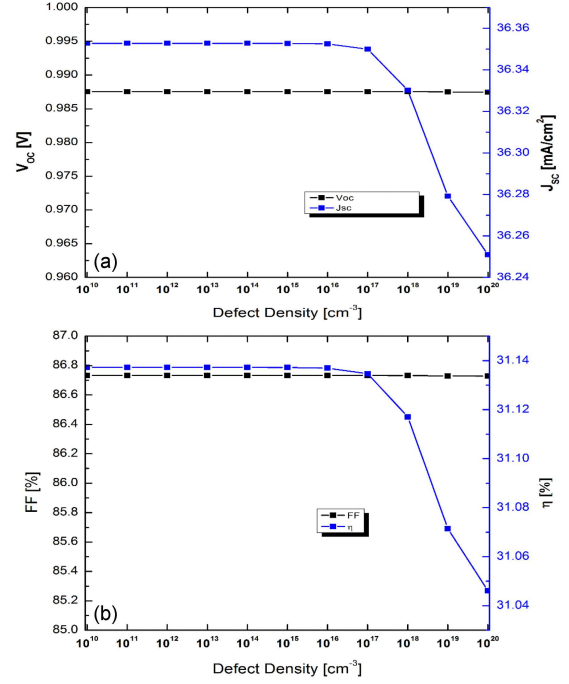


Fig. 10. The impact of AZO window layer defect density on solar cell performance (a) V_{oc} and J_{sc} variation, (b) FF and η variation.

The efficiency of around 31.14% is almost unaffected as defect density is increased from 10^{10} to 10^{17} cm⁻³. Then efficiency starts to decline. The efficiency decreases to 31.05% as defect density is increased to 10^{20} cm⁻³. Due to the AZO window layer's high doping concentration and bandgap compared to other layers used and thin thickness, the defect density of this layer has the least impact on solar cell performance [3]. Thus, AZO window layer defect density needs to be kept below 10^{17} cm⁻³.

3.10. Impact of CMTS/ZrS₂ interface defect density

The impact of CMTS/ZrS₂ interface defect density on solar cell performance is analyzed by altering the defect density from 10^8 to 10^{17} cm⁻². Neutral type defect is considered at the CMTS/ZrS₂ interface. The simulation results are shown in Fig. 11. Recombination centers are created by traps existing at the interface, which reduce carrier collection and efficiency [69]. It is observed that as interface defect density is increased, all solar cell parameters decrease. But if interface defect density increases above 10^9 cm⁻², the efficiency of the solar cell starts deteriorating significantly due to an increase in the series resistance of the cell [70]. So, for optimal solar cell performance, CMTS/ZrS₂ interface defect density needs to be minimized below 10^9 cm⁻². It has been explored that interface defect density of moderate value influences majorly solar cell performance [71].

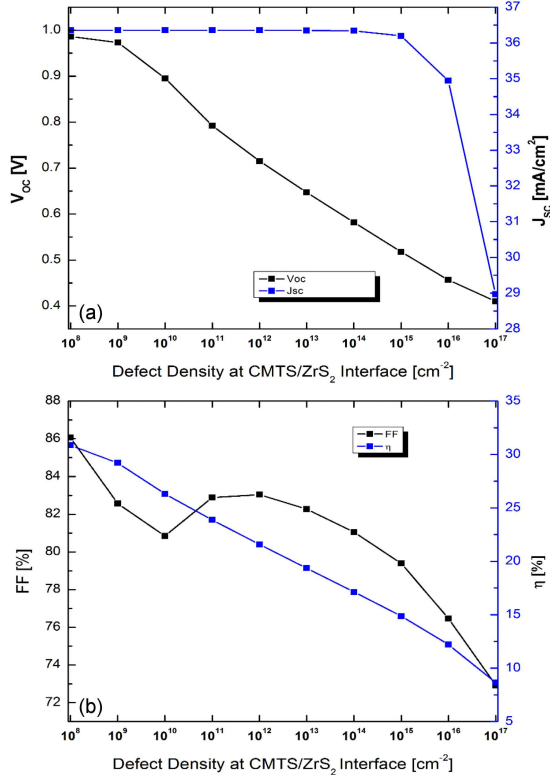


Fig. 11. The impact of CMTS/ZrS₂ interface defect density on solar cell performance (a) V_{oc} and J_{sc} variation, (b) FF and η variation.

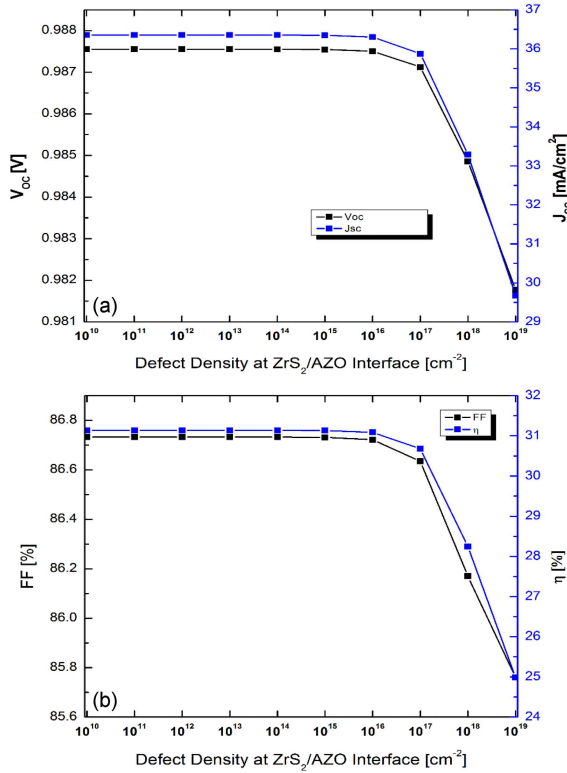


Fig. 12. The impact of ZrS₂/AZO interface defect density on solar cell performance (a) V_{oc} and J_{sc} variation, (b) FF and η variation.

3.11. Impact of ZrS₂/AZO interface defect density

The change in solar cell performance is explored by altering the defect density from 10¹⁰ to 10¹⁹ cm⁻² at the ZrS₂/AZO interface. Neutral type defect is considered at the ZrS₂/AZO interface. The simulation results are shown in Fig. 12. The efficiency close to 31.14% is almost unchanged as defect density is increased from 10¹⁰ to 10¹⁶ cm⁻². The efficiency of the solar cell starts to decrease significantly as defect density is increased above 10¹⁶ cm⁻². The efficiency diminishes to 24.98% as defect density is increased to 10¹⁹ cm⁻². Therefore, ZrS₂/AZO interface defect density needs to be minimized below 10¹⁶ cm⁻². It has been revealed that the performance parameters of the solar cell are less affected by the defects at the buffer/window interface than at the absorber/buffer interface. This is due to the high bandgap and donor concentration in the AZO window layer [3].

3.12. Impact of CMTS absorber layer electron affinity

The impact of CMTS absorber layer electron affinity on solar cell performance is analyzed by altering the electron affinity (EA) from 4 to 4.7 eV, and the results are shown in Fig. 13. As absorber

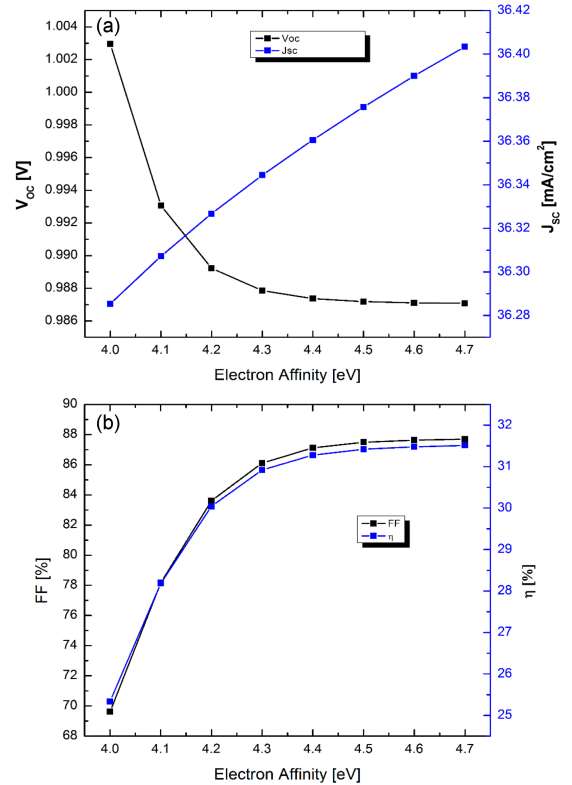


Fig. 13. The impact of CMTS absorber layer electron affinity on solar cell performance (a) V_{oc} and J_{sc} variation, (b) FF and η variation.

TABLE II
Optimized parameters and their values for
CMTS/ZrS₂/AZO thin-film solar cell.

| Optimized parameter | Value |
|--|-------------------------------------|
| CMTS absorber layer thickness | 2 μm |
| ZrS ₂ buffer layer thickness | 0.2 μm |
| AZO window layer thickness | 0.1 μm |
| CMTS absorber layer acceptor concentration | 10^{18} cm^{-3} |
| ZrS ₂ buffer layer donor concentration | 10^{19} cm^{-3} |
| CMTS absorber layer defect density | less than 10^{13} cm^{-3} |
| ZrS ₂ buffer layer defect density | less than 10^{16} cm^{-3} |
| AZO window layer defect density | less than 10^{17} cm^{-3} |
| CMTS/ZrS ₂ interface layer defect density | less than 10^9 cm^{-2} |
| ZrS ₂ /AZO interface defect density | less than 10^{16} cm^{-2} |
| CMTS absorber layer electron affinity | 4.7 eV |

layer electron affinity is increased from 4 to 4.7 eV, V_{oc} declines but both J_{sc} and FF increases. The cumulative effect of V_{oc} , J_{sc} , and FF causes efficiency to increase from 25.33 to 31.51% as electron affinity is increased from 4 to 4.7 eV. The conduction band offset (CBO) [$\text{CBO} = (\text{EA})_{\text{absorber}} - (\text{EA})_{\text{buffer}}$] is changed as the EA of the absorber layer is changed. The highest efficiency is obtained for EA of 4.7 eV, which results in CBO of 0 eV, which is within the range of optimal CBO of 0–0.3 eV, which reduces series resistance [72–74]. The chosen optimal CMTS absorber layer electron affinity is 4.7 eV.

3.13. Overall performance of optimized CMTS-based solar cell

The optimum parameters of various layers in the CMTS/ZrS₂/AZO solar cell are displayed in Table II. Using the optimized parameters of each layer, the solar cell efficiency of 31.54% with $V_{oc} = 0.99 \text{ V}$, $J_{sc} = 36.44 \text{ mA/cm}^2$, and $\text{FF} = 87.69\%$ is extracted from the simulated heterojunction solar cell.

4. Conclusions

In the present work, the CMTS/ZrS₂/AZO solar cell structure is modeled and simulated by the SCAPS-1D simulation software. Essential parameters like thicknesses, doping concentrations, electron

affinity, and defect density are analyzed. The optimized thicknesses for CMTS, ZrS₂, and AZO are 2 μm , 0.2 μm , and 0.1 μm , respectively, yielding a maximum efficiency of 31.54% ($V_{oc} = 0.99 \text{ V}$, $J_{sc} = 36.44 \text{ mA/cm}^2$, $\text{FF} = 87.69\%$) for the solar cell after optimization of shallow acceptor and donor density, defect density, and electron affinity. With the increase in defect density, the carrier recombination rate will increase, decreasing the carrier's lifetime and efficiency. CMTS defect density and CMTS/ZrS₂ interface defect density are observed to reduce cell performance because of their significant contribution to the series resistance of the cell. The optimized 4.7 eV electron affinity of the CMTS absorber layer results in zero conduction band offset, which is favorable for the charge carriers traveling to the metal contact by avoiding recombination and enhances efficiency. The light is effectively absorbed by the optimized CMTS-based solar cell, resulting in the creation of carriers that separate quickly with minimal bulk recombination with high values of FF and J_{sc} . Due to low lattice mismatch and interfacial defects, recombination at the interface decreases and results in a high V_{oc} value. As a consequence, due to the combined effect of V_{oc} , J_{sc} , and FF, a high efficiency of 31.54% is achieved, which is close to the maximum efficiency of 32.5% according to the Shockley–Queisser limit for 1.2 eV bandgap CMTS absorber layer. This work will contribute to the fabrication of high-efficiency CMTS-based solar cells in the near future.

Acknowledgments

The author would like to thank Dr. Marc Burgelman at the Department of Electronics and Information Systems, University of Gent, Belgium, for providing the SCAPS software package.

References

- [1] M.A. Rahman, *Opt. Mater. Express* **12**, 2954 (2022).
- [2] M. Abdelfatah, A.M.E. Sayed, W. Ismail, S. Ulrich, V. Sittinger, A. El-Shaer, *Sci. Rep.* **13**, 4553 (2023).
- [3] A. Isha, A. Kowsar, A. Kuddus, M.K. Hosain, M.H. Ali, M.D. Haque, M.F. Rahman, *Heliyon* **9**, e15716 (2023).
- [4] X. Chen, J. Liu, J. Feng, E. Zhang, H. Wang, X. Liu, J. Liu, H. Rong, M. Xu, J. Zhang, *J. Mater. Chem. A* **6**, 11898 (2018).
- [5] K.V. Gurav, S.W. Shin, U.M. Patil, M.P. Suryawanshi, S.M. Pawar, M.G. Gang, S.A. Vanalakar, J.H. Yun, J.H. Kim, *J. Alloys Compd.* **631**, 178 (2015).

- [6] K. Woo, K. Kim, Z. Zhong, I. Kim, Y. Oh, S. Jeong, J. Moon, *Sol. Energy Mater. Sol. Cells* **128**, 362 (2014).
- [7] J. Krustok, T. Raadik, M. Grossberg, S. Giraldo, M. Neuschitzer, S. Lopez-Marino, E. Saucedo, *Mater. Sci. Semicond. Process.* **39**, 251 (2015).
- [8] G. Brammertz, M. Buffie, M. Meuris, J. Poortmans, K.B. Messaoud, S. Sahayaraj, C. Köble, M. Meuris, J. Poortmans, *Appl. Phys. Lett.* **103**, 163904 (2013).
- [9] S. Delbos, *EPJ Photovolt.* **3**, 35004 (2012).
- [10] C. Platzer-Bjorkman, J. Scragg, H. Flamersberger, T. Kubart, M. Edoff, *Sol. Energy Mater. Sol. Cells* **98**, 110 (2012).
- [11] C. Persson, *J. Appl. Phys.* **107**, 053710 (2010).
- [12] M. Ravindiran, C. Praveenkumar, *Renew. Sust. Energy Rev.* **94**, 317 (2018).
- [13] H. Wei, W. Guo, Y. Sun, Z. Yang, Y. Zhang, *Mater. Lett.* **64**, 1424 (2010).
- [14] K. Tanaka, N. Moritake, H. Uchiki, *Sol. Energy Mater. Sol. Cells* **91**, 1199 (2007).
- [15] A. Haddout, A. Raidou, M. Fahoume, *Appl. Phys. A* **125**, 124 (2019).
- [16] A.D. Adewoyin, M. Olopade, M.A. Chendo, *Optik* **133**, 122 (2017).
- [17] S. Vallisree, R. Thangavel, T.R. Lenka, *J. Mater. Sci. Mater.* **29**, 7262 (2018).
- [18] S.R. Meher, L. Balakrishanan, Z.C. Alex, *Superlattices Microstruct.* **100**, 703 (2016).
- [19] F.Z. Nainaa, H. Ez-Zahraouy, *Comput. Condens. Matter* **16**, e00321 (2018).
- [20] K. Rudisch, W.F. Espinosa-García, J.M. Osorio-Guillen, C.M. Araujo, C. Platzer-Bjorkman, J.J.S Scragg, *Phys. Status Solidi B* **256**, 1800743 (2019).
- [21] Z. Tong, J. Yuan, J. Chen et al., *Mater. Lett.* **237**, 130 (2019).
- [22] S. Sharma, P. Kumar, *J. Phys. Commun.* **1**, 045014 (2017).
- [23] S. Rondiya, N. Wadnerkar, Y. Jadhav, S. Jadkar, S. Haram, M. Kabir, *Chem. Mater.* **29**, 3133 (2017).
- [24] M.A. Green, E.D. Dunlop, D.H. Levi, J. Hohl-Ebinger, M. Yoshita, A.W.Y. Ho-Baillie, *Prog. Photovolt. Res. Appl.* **27**, 565 (2019).
- [25] A. Ziti, B. Hartiti, A. Belafhaili, H. Labrim, S. Fadili, A. Ridah, M. Tahri, P. Thevenin, *Appl. Phys. A* **127**, 1 (2021).
- [26] A.J. Salh, N.A. Bakr, *Chalcogenide Lett.* **19**, 483 (2022).
- [27] R.R. Prabhakar, S. Zhenghua, Z. Xin, T. Baikie, L.S. Woei, S. Shukla, S.K. Batabyal, O. Gunawan, L.H. Wong, *Sol. Energy Mater. Sol. Cells* **157**, 867 (2016).
- [28] L. Chen, H. Deng, J. Tao, H. Cao, L. Sun, P. Yang, J. Chu, *Acta Mater.* **109**, 1 (2016).
- [29] J. Jean, P.R. Brown, R.L. Jaffe, T. Buonassisi, V. Bulovic, *Energy Environ. Sci.* **8**, 1200 (2015).
- [30] J. Yu, H. Deng, L. Chen, J. Tao, Q. Zhang, B. Guo, L. Sun, P. Yang, X. Zheng, J. Chu, *Mater. Chem. Phys.* **211**, 382 (2018).
- [31] X. Wang, T. Liu, F. Yu, H. Hou, *J. Optoelectron. Adv. Mater.* **13**, 7 (2019).
- [32] L. Chen, H. Deng, J. Tao, W. Zhou, L. Sun, F. Yue, P. Yang, J. Chu, *J. Alloys Compd.* **640**, 23, (2015).
- [33] S. Marchionna, A.L. Donne, M. Merlini, S. Binetti, M. Acciarri, F. Cernuschi, *J. Alloys Compd.* **693**, 95 (2017).
- [34] T. Pansuriya, R. Malani, V. Kheraj, *Opt. Mater.* **126**, 112150 (2022).
- [35] Y.H. Khattak, F. Baig, B. Marí, S. Beg, S. Ahmed, *J. Nanoelectron. Optoelectron.* **13**, 1678 (2018).
- [36] M. Patel, P.M. Pataniya, V. Patel, C.K. Sumesh, D. Late, *Sol. Energy* **206**, 974 (2020).
- [37] C. Gautam, A. Verma, P. Chaudhary, B.C. Yadav, *Opt. Mater.* **123**, 111860 (2022).
- [38] M. Moustafa, T.A. Zoubi, S. Yasin, *Opt. Mater.* **124**, 112001 (2022).
- [39] Y. Li, H. Wang, B. Chang, Y. Guo, Z. Li, S.H. Talib, Z. Lu, J. Wang, *Green Energy Environ.* **8**, 1174 (2022).
- [40] L. Li, H. Wang, X. Fang, T. Zhai, Y. Bando, D. Golberg, *Energy Environ. Sci.* **4**, 2586 (2011).
- [41] T.V. Vu, A.A. Lavrentyev, D.V. Thuan et al., *Superlattices Microstruct.* **125**, 205 (2019).
- [42] M. Hamada, K. Matsuura, T. Hamada, I. Muneta, K. Kakushima, K. Tsutsui, H. Wakabayashi, *Jpn. J. Appl. Phys.* **60**, SBBH05 (2021).
- [43] Y. Tian, Y. Cheng, J. Huang, S. Zhang, H. Dong, G. Wang, J. Chen, J. Wu, Z. Yin, X. Zhang, *Nano Res.* **15**, 6628 (2022).
- [44] M. Hamada, K. Matsuura, T. Sakamoto, I. Muneta, T. Hoshii, K. Kakushima, K. Tsutsui, H. Wakabayashi, *IEEE J. Electron Devices Soc.* **7**, 1258 (2019).
- [45] M. Mattinen, P.J. King, G. Popov, J. Hämäläinen, M.J. Heikkilä, M. Leskelä, M. Ritala, *2D Mater.* **7**, 011003 (2019).

- [46] Y. Shimazu, Y. Fujisawa, K. Arai, T. Iwabuchi, K. Suzuki, *ChemNanoMat* **4**, 1078 (2018).
- [47] S.K. Swami, J.I. Khan, V. Dutta, J. Lee, F. Laquai, N. Chaturvedi, *ACS Appl. Energy Mater.* **6**, 2906 (2023).
- [48] M. Krajewski, M. Tokarczyk, P. Świętochowski, P. Wróbel, M. Kaminěska, A. Drabiněska, *ACS Omega* **8**, 30621 (2023).
- [49] M.W. Alam, M.Z. Ansari, M. Aamir, M. Waheed-Ur-Rehman, N. Parveen, S.A. Ansari, *Crystals* **12**, 128 (2022).
- [50] L. Vinet, A. Zhedanov, *J. Phys. A Math. Theor.* **44**, 085201 (2011).
- [51] Y.H. Khatlak, F. Baig, S. Ullah, B. Mari, S. Beg, H. Ullah, *J. Renew. Sustain. Energy* **10**, 033501 (2018).
- [52] C.Y. Tsay, W.T. Hsu, *Materials* **10**, 1379 (2017).
- [53] Z.R. Zapukhlyak, L.I. Nykyruy, V.M. Rubish, G. Wisz, V.V. Prokopiv, M.O. Galushchak, I.M. Lishchynskyy, L.O. Katanova, R.S. Yavorsky, *Phys. Chem. Solid State* **21**, 660 (2020).
- [54] A.Srivastava, P. Dua, T.R. Lenka, S.K. Tripathy, *Mater. Today Proc.* **43**, 3735 (2021).
- [55] W. Shockley, H.J. Queisser, *J. Appl. Phys.* **32**, 510 (1961).
- [56] J.C.Z. Medina, E.R. Andres, C.M. Ruíz et al., *Heliyon* **9**, e14547 (2023).
- [57] A. Bouarissa, A. Gueddim, N. Bouarissa, H. Maghraoui-Meherezi, *Mater. Sci. Eng. B* **263**, 114816 (2021).
- [58] A.J. Salh, N.A. Bakr, *Chalcogenide Lett.* **19**, 483 (2022).
- [59] Y.E. Romanyuk, S.G. Haass, S. Giraldo et al., *J. Phys. Energy* **1**, 044004 (2019).
- [60] R.R. Prabhakar, S. Zhenghua, Z. Xin, T. Baikie, L.S. Woei, S. Shukla, S.K. Batabyal, O. Gunawan, L.H. Wong, *Sol. Energy Mater. Sol. Cells* **157**, 867 (2016).
- [61] M.H. Ali, M.A.A. Mamun, M.D. Haque, M.F. Rahman, M.K. Hossain, A.Z.M.T. Islam, *ACS Omega* **8**, 7017 (2023).
- [62] W. Henni, W.L. Rahal, D. Rached, *Acta Phys. Pol. A* **142**, 445 (2022).
- [63] K.T. Arockiya-Dass, K. Sekar, L. Marasamy, *Energy Technol.* **11**, 2300333 (2023).
- [64] S.Taheri, A.A. Kordbacheh, M. Minbashi, A. Hajjiah, *Opt. Mater.* **111**, 110601 (2021).
- [65] A. Khadir, *Acta Phys. Pol. A* **137**, 1128 (2020).
- [66] M.F. Rahman, N. Mahmud, I. Alam, M.H. Ali, M.M.A. Moon, A. Kuddus, G.F.I. Toki, M.H.K. Rubel, M.A.A. Asad, M.K. Hossain, *AIP Adv.* **13**, 045309 (2023).
- [67] R. Kondrotas, C. Chen, X.X. Liu, B. Yang, J. Tang, *J. Semicond.* **42**, 031701 (2021).
- [68] F.Y. Ran, Z. Xiao, Y. Toda, H. Hiramatsu, H. Hosono, T. Kamiya, *Sci. Rep.* **5**, 10428 (2015).
- [69] M.S.S. Basyoni, M.M. Salah, M. Mousa, A. Shaker, A. Zekry, M. Abouelatta, M.T. Alshammari, K.A. Al-Dhlan, C. Gontrand, *IEEE Access* **9**, 130221 (2021).
- [70] S. Ahmmed, A. Aktar, J. Hossain, A.B.M. Ismail, *Sol. Energy* **207**, 693 (2020).
- [71] V. Mishra, C.Tiwari, R. Chauhan, *IOP Conf. Ser. Earth Environ. Sci.* **1084**, 012004 (2022).
- [72] A. Barkhouse, R. Haight, N. Sakai, H. Hiroi, H. Sugimoto, D.B. Mitzi, *Appl. Phys. Lett.* **100**, 193904 (2012).
- [73] T. Minemoto, T. Matsui, H. Takakura, Y. Hamakawa, T. Negami, Y. Hashimoto, T. Uenoyama, M. Kitagawa, *Sol. Energy Mater. Sol. Cells* **67**, 83 (2001).
- [74] J. Yu, Z. Zheng, L. Dong, S. Cheng, Y. Lai, Q. Zheng, H. Zhou, H. Jia, H. Zhang, *Chin. Phys. B* **26**, 046802 (2017).